

Plasticity-Induced Growth of Dendritic Spines by Exocytic Trafficking from Recycling Endosomes

Mikyong Park,¹ Jennifer M. Salgado,³
Linnaea Ostroff,³ Thomas D. Helton,¹
Camenzind G. Robinson,^{1,2} Kristen M. Harris,^{3,4}
and Michael D. Ehlers^{1,2,*}

¹Department of Neurobiology

²Howard Hughes Medical Institute
Duke University Medical Center
Durham, North Carolina 27710

³Department of Neurology, Synapses and
Cognitive Neuroscience Center
Medical College of Georgia
Augusta, Georgia 30912

⁴Center for Learning and Memory
Section of Neurobiology
The University of Texas at Austin
Austin, Texas 78712

Summary

Dendritic spines are micron-sized membrane protrusions receiving most excitatory synaptic inputs in the mammalian brain. Spines form and grow during long-term potentiation (LTP) of synaptic strength. However, the source of membrane for spine formation and enlargement is unknown. Here we report that membrane trafficking from recycling endosomes is required for the growth and maintenance of spines. Using live-cell imaging and serial section electron microscopy, we demonstrate that LTP-inducing stimuli promote the mobilization of recycling endosomes and vesicles into spines. Preventing recycling endosomal transport abolishes LTP-induced spine formation. Using a pH-sensitive recycling cargo, we show that exocytosis from recycling endosomes occurs locally in spines, is triggered by activation of synaptic NMDA receptors, and occurs concurrently with spine enlargement. Thus, recycling endosomes provide membrane for activity-dependent spine growth and remodeling, defining a novel membrane trafficking mechanism for spine morphological plasticity and providing a mechanistic link between structural and functional plasticity during LTP.

Introduction

Dendritic spines are micron-sized membrane protrusions of neuronal dendrites that are the major sites of contact for glutamatergic presynaptic inputs in the mammalian central nervous system (Hering and Sheng, 2001). Spines are motile and assume diverse shapes, which are correlated with synaptic strength (Matsuzaki et al., 2001). Further, spine morphology is subject to rapid alteration by patterns of neuronal activity and postsynaptic glutamate receptor activation (Lang et al., 2004; Matsuzaki et al., 2004). Recent studies have found that new spines form and existing spines grow in re-

sponse to stimuli that induce long-term potentiation (LTP) in the hippocampus (Engert and Bonhoeffer, 1999; Maletic-Savatic et al., 1999; Lang et al., 2004; Matsuzaki et al., 2004), the dominant cellular model for learning and memory (Malenka and Nicoll, 1999). Such structural growth and expansion of dendritic spines has served as a paradigmatic cellular model for physical alteration of neural circuitry during learning-related plasticity. Along with spine growth, morphological changes associated with LTP include enlargement of the postsynaptic density (PSD) (Toni et al., 1999), remodeling of spine actin (Okamoto et al., 2004), redistribution of polyribosomes (Ostroff et al., 2002) and mitochondria (Li et al., 2004), and the appearance of intraspinous vesicles (Toni et al., 2001). The latter observation points to the possibility for spatially regulated membrane trafficking events during spine growth. However, to date, emphasis has been placed on spine morphological plasticity through remodeling of the actin cytoskeleton (Tada and Sheng, 2006). Interestingly, linkage of the actin cytoskeleton to the plasma membrane through the protein kinase C target MARCKS maintains spine morphology (Calabrese and Halpain, 2005). However, the source of membrane for increased spine volume and new spine formation during LTP has been unknown.

Membrane for spine expansion could be provided by lateral plasma membrane of the dendritic shaft or by fusion of intracellular membrane compartments. Dendrites are rich in internal membrane compartments including extensive smooth endoplasmic reticulum (Spacek and Harris, 1997), sparse Golgi elements (Horton et al., 2005), and endosomes (Cooney et al., 2002) whose function and molecular identity remain poorly characterized. In nonneuronal cells, membrane traffic through endosomes contributes to cell morphogenesis. In migrating chick embryo fibroblasts, the transferrin (Tf) receptor (TfR), a representative fast and constitutive recycling transmembrane protein, is loaded into perinuclear recycling endosomes and then trafficked to the surface of the leading lamella (Hopkins et al., 1994). In addition, membrane accumulation for cleavage furrow growth during the terminal phase of cytokinesis in the early *Caenorhabditis elegans* embryo is dependent on Rab11 (Skop et al., 2001), a small GTPase required for membrane transport from the recycling endosome to the plasma membrane (Ullrich et al., 1996). Finally, disruption of the *Drosophila* exocyst components sec5, sec6, and sec15 in epithelial cells causes accumulation of E-cadherin in an enlarged recycling endosomal compartment and inhibits its delivery to the plasma membrane (Langevin et al., 2005). Such studies suggest that cellular membrane microdomain composition and shape is governed by rates of endocytosis to and exocytosis from endosomes aligned through the endocytic recycling pathway.

At excitatory synapses on dendritic spines, postsynaptic membrane composition is subject to continuous regulation by endocytic cycling of neurotransmitter receptors (Ehlers, 2000). Continuous endocytosis of postsynaptic molecules occurs at specialized endocytic zones on spines lateral to the PSD (Blanpied et al.,

*Correspondence: ehlers@neuro.duke.edu

2002). Given the small size of dendritic spines, endocytic or exocytic events could have a significant impact on spine size. Yet, in the absence of plasticity-inducing stimuli, most spines are structurally stable (Grutzendler et al., 2002), suggesting precise spatial control over membrane recycling. Notably, recycling endosomes are highly dynamic in hippocampal neuron dendrites (Prekeris et al., 1999). Moreover, ultrastructural analysis has revealed a widespread pool of recycling compartments and vesicles that serve multiple dendritic spines (Cooney et al., 2002), potentially positioning endosomes to provide membrane and molecular material to specific spine microdomains.

During LTP, the number of AMPA-type glutamate receptors at the plasma membrane increases due to enhanced transport from recycling endosomes (Park et al., 2004). This increase in postsynaptic AMPA receptors produces an increase in AMPA receptor-mediated transmission (Shi et al., 1999). In addition, LTP-inducing stimuli increase the abundance of coated vesicles in spines (Toni et al., 2001) and increase the rate of recycling endosome transport (Park et al., 2004). These results point to the possibility that enhanced recycling not only ensures enhanced synaptic efficacy by providing AMPA receptors but also mediates spine growth and structural remodeling by supplying lipid membrane and other unknown proteins, thereby coupling membrane remodeling with synaptic potentiation. Yet, little is known about where the relevant endosomal compartments reside in dendrites and spines, whether exocytic events from recycling endosomes occur within spines, and how membrane trafficking from endosomes is regulated during plasticity-associated spine growth.

In this study, we have investigated the effect of recycling endosome transport on spine growth and maintenance and the regulation of such transport by LTP-inducing stimuli. Using a combination of live-cell imaging, electron microscopy, and direct visualization of exocytosis from dendritic endosomes, we demonstrate that transport from recycling endosomes bidirectionally regulates spine formation and loss. During LTP, recycling endosomes and endosomal vesicles are rapidly mobilized into spines. Disruption of recycling endosome transport leads to acute spine collapse and prevents LTP-induced spine formation. Exocytosis of cargo from recycling endosomes occurs locally within dendritic spines, is triggered by activation of synaptic NMDA receptors, and occurs concurrently with spine enlargement. These results demonstrate a novel requirement for intracellular membrane trafficking in spine morphogenesis, provide direct evidence for local exocytosis in spines, and identify recycling endosomes as the source of membrane material for activity-dependent spine growth. Activity-dependent establishment of local endosomal recycling provides a potential mechanism linking structural and functional plasticity of highly compartmentalized dendritic spines.

Results

Recycling Endosomes Are Positioned Near Dendritic Spines

To determine the spatial relation of recycling endosomes to dendritic spines, we labeled recycling endo-

somes in hippocampal neurons (DIV17) using either fluorophore-conjugated transferrin (Alexa-Tf) uptake or immunocytochemical detection of the recycling endosome marker proteins transferrin receptor (TfR), Rab11, and syntaxin13. Recycling endosomes were present in the dendritic shaft and also appeared in spines (Figure 1A). Within the dendritic shaft, recycling endosomes were frequently positioned at the base of spines near the origin of the spine neck (Figures 1B and 1C). Quantitative analysis revealed that most spines had recycling endosomes at their base (a; Figures 1B and 1C), while some spines had recycling endosomes in their neck (b; Figures 1B and 1C) or in their spine head (c; Figures 1B and 1C). A few spines had endosomes extending from the dendritic shaft into the spine neck (a + b; Figure 1B). Notably, less than 10% of spines lacked recycling endosomes in either the spine proper or in immediately adjacent regions of the dendritic shaft.

To examine and quantify spine endosomes in more intact circuits in situ, we performed serial section transmission electron microscopy (sSTEM) in postnatal day 15 (PN15) dendrites from acute rat hippocampal slices. Endosomal compartments were categorized into recycling compartments (RCs; red; Figure 1D, panels D1 and D3i) with or without a multivesicular body (MVB; blue; Figure 1D, panels D1 and D3i), amorphous vesicular clumps (AVCs; green; Figure 1D, panel D2), and free endosomes (including abundant smooth vesicles marked with yellow and occasional coated vesicles marked with orange) as previously described (Cooney et al., 2002). RCs contained tubules with and without coated buds and smooth and coated vesicles. RCs were found both with and without an associated MVB (blue; Figure 1D, panels D1 and D3i). AVCs were distinguished from RCs by their irregular shape and absence of coated vesicles or tubules. In previous studies, all of these compartments (RCs, AVCs, and free endosomes) contained gold-conjugated cargo endocytosed from the extracellular space, which distinguished them from smooth endoplasmic reticulum, which never contained gold particles (Cooney et al., 2002). These endosomal compartments were distributed at the base (a, 56.8% of spines; Figure 1E), in the neck (b, 40.4% of spines; Figure 1E), and in the head (c, 50% of spines; Figure 1E) of dendritic spines (Figure 1E). Pre-embedding immunogold electron microscopy of adult rat CA1 hippocampus revealed TfR-positive membrane compartments at the base, in the neck, and in the head of dendritic spines, which had morphological characteristics indistinguishable from endosomal compartments identified by sSTEM (Figure 1F). Thus, under basal conditions in primary neuron cultures, hippocampal slices, and adult rat brain, endosomes are poised immediately beneath spines or in the spine head proper, suggesting rapid availability of recycling cargo for membrane plasticity.

Internal Endosomal Membranes Equal a Significant Fraction of Spine Surface Area

Next, we considered whether endosomes localized within or near spines (Figure 1) have enough membrane to contribute to spine growth or maintenance. Membrane surface areas of spines and endosomal compartments were measured through serial sections (Figures 2A and 2B). The membranes of all tubules and

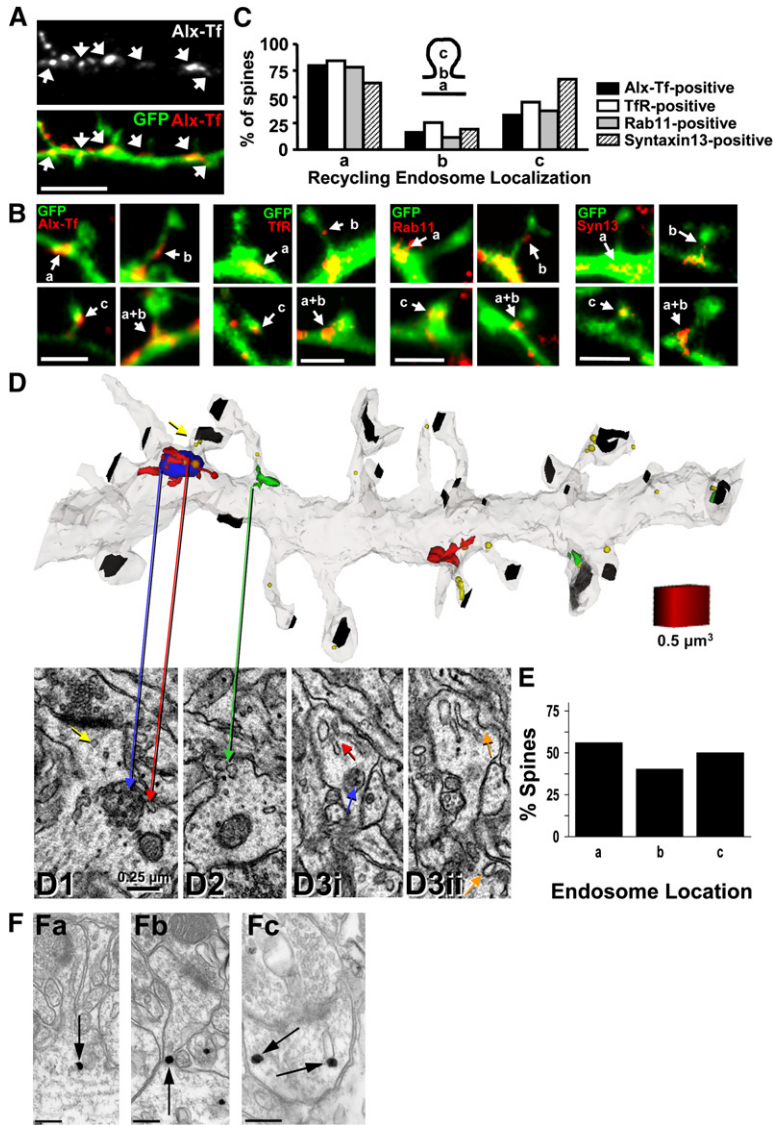


Figure 1. Recycling Endosomes Localize within or at the Base of Dendritic Spines

(A) Distribution of recycling endosomes in dendrites and spines. Hippocampal neurons (DIV17) expressing GFP were incubated with Alexa-Tf (100 $\mu\text{g/ml}$; Alexa-Tf) for 1 hr at 37°C to label recycling endosomes. Arrows indicate Alexa-Tf-labeled recycling endosomes in dendrites. Note the localization of recycling endosomes either within spines or at the base of spines in the dendritic shaft. Scale bar, 5 μm .

(B) Representative images showing the localization of recycling endosomes containing Alexa-Tf, transferrin receptor (Tfr), Rab11, or syntaxin13 (Syn13) in spines. Letters indicate the location code illustrated in (C). Scale bars, 2 μm .

(C) Proportion of spines containing recycling endosomes in the indicated locations. $n = 157, 150, 128,$ and 182 spines analyzed from 12, 11, 9, and 8 neurons for Alexa-Tf-, Tfr-, Rab11-, and syntaxin13-positive compartments, respectively. Note that values do not add up to 100%, as individual spines could fall into more than one category.

(D) Top, three-dimensional (3D) reconstruction from sSTEM illustrating endosomal compartments from acute hippocampal slices (PN15). Recycling compartments (RCs; red), multivesicular bodies (MVBs; blue), amorphous vesicular clumps (AVCs; green), and free endosomes (yellow, smooth vesicles; orange, coated vesicles) in spines are illustrated. Postsynaptic densities are labeled in black. Bottom, thin sections through individual spines containing a RC (red arrow; [D1]), an AVC at the base (green arrow; [D2]), or adjacent serial thin sections (D3i and D3ii) through a dendritic spine containing a large RC (red arrow; [D3i]), a MVB (blue arrow; [D3i]), and coated pits both on the head and at the base of the spine (orange arrows; [D3ii]). Arrows are color-coded to match the 3D reconstruction. Scale cube (0.5 μm^3) is shown in the upper panel. Scale bar in (D1) applies to (D1)–(D3).

(E) Percentage of spines containing endosomal

compartments within 0.1 μm of the base (a), in the neck (b) or in the head (c) of spines. $n = 14$ dendritic segments with an average length of 8.5 μm .

(F) Immunogold localization of transferrin receptor (Tfr) at dendritic spines in adult rat CA1 hippocampus. Arrows indicate Tfr-positive endosomes at the base (Fa), in the neck (Fb), and in the head (Fc) of spines. Scale bars, 200 nm.

vesicles in both RCs (red; **Figures 2Aii** and **2Bii**) and AVCs (green; **Figure 2Bii**) were measured, excluding the membrane of MVBs. Quantitative analysis revealed that the range in membrane surface area of dendritic spines overlapped substantially with the surface area summed across vesicles and tubules in RCs or AVCs (mean surface area: spines, 0.66 μm^2 ; RC, 0.35 μm^2 ; AVC, 0.43 μm^2 ; **Figure 2C**). Moreover, spines containing endosomal compartments were larger than spines lacking endosomes (**Figure 2D**). Thus, the summed membrane area of RCs or AVCs is a substantial fraction of the spine membrane surface area, revealing a correlation between the presence of endosomes and spine size.

Transport from Recycling Endosomes Maintains Dendritic Spines

We next measured the effect of blocking recycling endosome transport on spine number by expressing either

a mutant version of the Eps15-homology domain protein EHD1/Rme1 (Rme1-G429R), a constitutively inactive GDP-bound form of the small GTPase Rab11a (Rab11a-S25N), or a soluble fragment of the recycling endosome SNARE protein syntaxin13 (Syn13 ΔTM) that forms cognate SNARE complexes but blocks membrane fusion due to its inability to bind membranes (**Figure 3A**) (**Lin et al., 2001; Park et al., 2004**). To visualize neuronal morphology, we filled neurons by expressing mRFP. In hippocampal neurons, blocking endocytic recycling markedly reduced the number of dendritic protrusions, most of which were spines (protrusions per 10 μm dendrite: GFP, 3.7 ± 0.1 ; Rme1-G429R, 1.8 ± 0.1 ; Rab11a-S25N, 1.8 ± 0.2 ; Syn13 ΔTM , 2.3 ± 0.1 ; **Figures 3B** and **3C**). Conversely, expression of wild-type Rme1, Rab11a, or syntaxin13 enhanced recycling (data not shown) and markedly increased total protrusion number (protrusions per 10 μm dendrite: Rme1-WT, 7.6 ± 0.4 ;

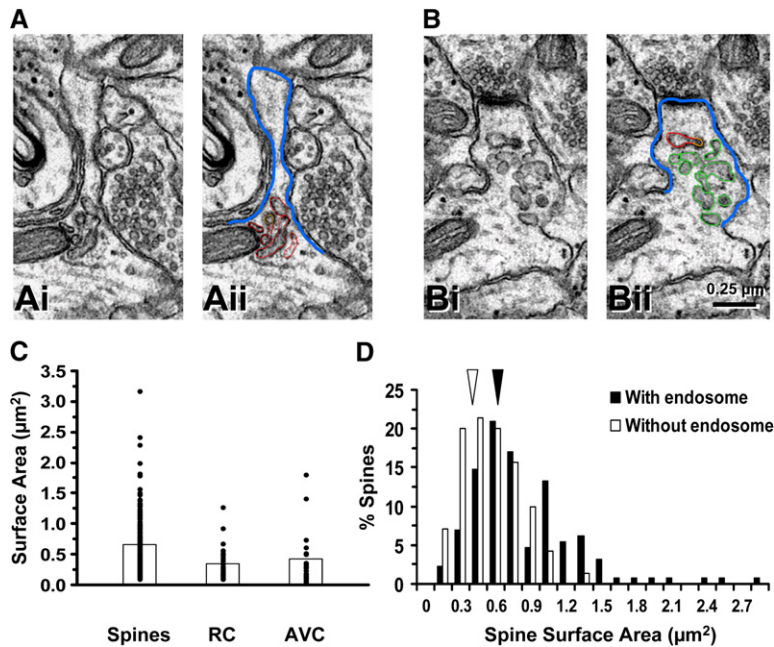


Figure 2. The Surface Area of Endosomal Compartments Is a Large Fraction of the Total Spine Surface Area

(A and B) Thin section images illustrating how the membrane surface for spines (blue lines in [Aii] and [Bii]), recycling endosomes (red lines in [Aii] and [Bii]), or amorphous vesicular clumps (green lines in [Bii]) was traced to measure membrane surface area. Scale bar in [Bii] applies to all panels.

(C) Median with superimposed values of surface areas for individual spines (Spines), recycling endosomes (RC), or amorphous vesicular clumps (AVC).

(D) Histograms of spine surface area. Arrows indicate median values. For (C) and (D), $n = 14$ dendritic segments with an average length of $8.5 \mu\text{m}$.

Rab11a-WT, 8.0 ± 0.5 ; Syntaxin13-WT, 7.0 ± 0.3 ; Figures 3B and 3C). These findings indicate that transport from recycling endosomes bidirectionally regulates spine number, and ongoing membrane trafficking from recycling endosomes is required to maintain spines.

Rapid Spine Loss upon Acute Inhibition of Recycling Endosome Transport

To rule out effects of chronic disruption of endocytic recycling, we applied a cell-permeable Syn13ΔTM fusion protein bearing the short acidic cell-penetrating TAT sequence to allow for cell entry. Purified Syn13ΔTM containing the TAT sequence (TAT-Syn13ΔTM, $3.5 \mu\text{M}$) was taken up into cultured hippocampal neurons in a time-dependent manner that was maximal after 60–90 min (see Figure S1 in the Supplemental Data available online). As a control, a purified TAT-fused soluble fragment of the late endosome SNARE protein syntaxin-7 (TAT-Syn7ΔTM, $3.5 \mu\text{M}$) (Sun et al., 2003) showed similar transducibility into hippocampal neurons (Figure S1). By following the trafficking of the recycling cargo Alexa-transferrin or the late endosomal trafficked cargo fluo-rescein-EGF, we confirmed that acute application of TAT-Syn13ΔTM or TAT-Syn7ΔTM blocked endocytic recycling and degradation, respectively (Figures S2 and S3).

To test whether acute blockade of recycling transport influences spine morphology, we performed time-lapse imaging of hippocampal neurons expressing tdTomato as a cell fill and applied Alexa-488-labeled TAT-Syn13ΔTM (Alexa-488-TAT-Syn13ΔTM; $3.5 \mu\text{M}$). Uptake of TAT-Syn13ΔTM proteins was confirmed by Alexa-488 fluorescence. During baseline imaging, dendritic protrusions were largely stable with the occasional appearance of new dendritic protrusions and loss of existing dendritic protrusions that balanced one another producing no net effect on protrusion number over the duration of the experiment under control conditions. However, following application of TAT-Syn13ΔTM, the total num-

ber of dendritic protrusions abruptly declined over 30–60 min (Figures 3D–3F) corresponding to the time course of TAT-Syn13ΔTM uptake (Figure S1). Conversely, application of TAT-Syn7ΔTM had no effect on spine number (Figure 3G). These data provide strong evidence that membrane cycling between recycling endosomes and the spine plasma membrane is continuous and rapid and that ongoing membrane trafficking from recycling endosomes is required to maintain spines.

Chemical LTP Stimuli Increase the Number and the Size of Spines in Cultured Hippocampal Neurons

We next wondered whether membrane trafficking from recycling endosomes provides a potential source of membrane and other proteins for spine remodeling. To this end, we first tested whether activation of synaptic NMDA receptors by glycine stimulation, a protocol used to induce chemical LTP in cultured hippocampal neurons (Lu et al., 2001; Park et al., 2004), elicits morphological changes associated with LTP such as spine enlargement and formation. We found that brief glycine stimulation markedly increased the number of spines and the size of preexisting spines (Figure 4A). Time-lapse imaging revealed that both the number of dendritic protrusions (Figures 4B and 4C; Movie S1) and the size of preexisting dendritic protrusions (Figures 4F and 4G; Movie S2) increased rapidly following glycine application. Both glycine-induced spine formation and preexisting spine growth were blocked by application of the NMDA receptor antagonist D-AP5 (Gly + AP5; Figures 4C and 4G), indicating that the increase in dendritic protrusion number and size was dependent on the activation of NMDA receptors (Engert and Bonhoeffer, 1999; Matsuzaki et al., 2004). Consistent with previous studies (Matsuzaki et al., 2004), the fractional increase of spine size was larger for small spines ($<0.85 \mu\text{m}^2$) than for large spines ($>0.85 \mu\text{m}^2$) (Figure S4A), while the absolute increase of spine size was nearly identical between small and large spines (Figure S4B). Thus, the absolute

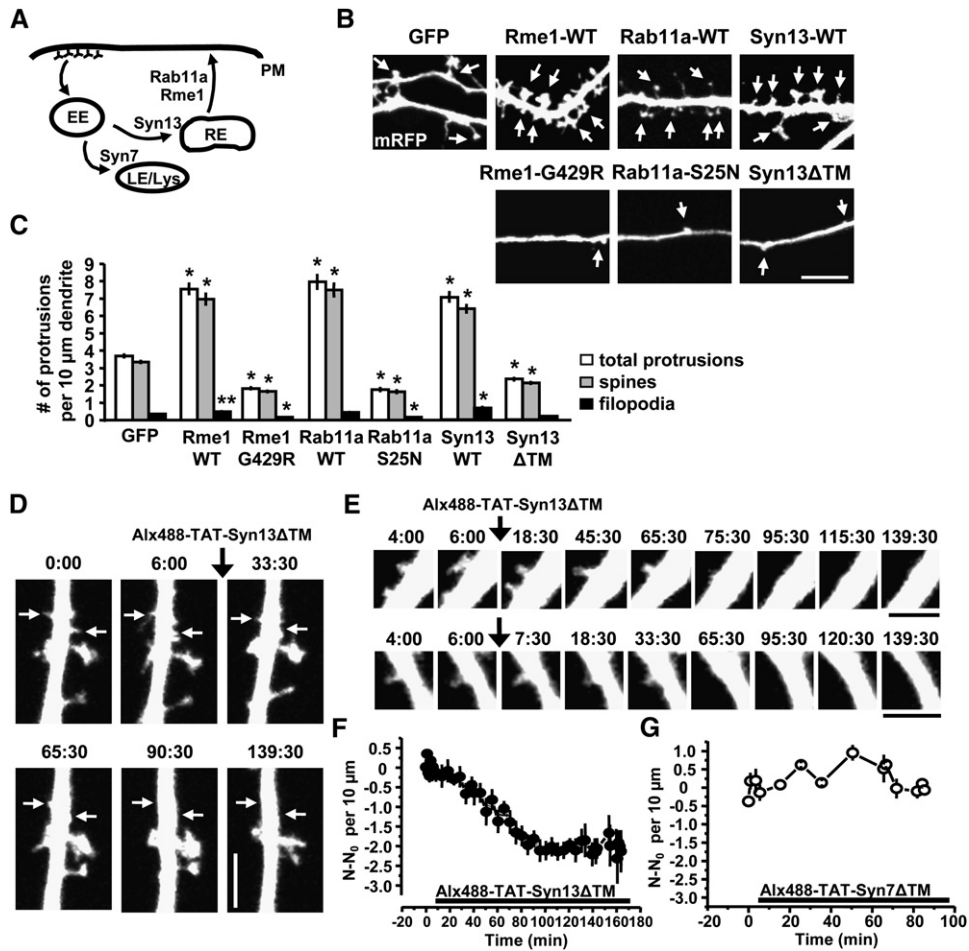


Figure 3. Maintenance of Dendritic Spines Requires Ongoing Transport from Recycling Endosomes

(A) Schematic diagram showing pathways of early and late endocytic trafficking between the plasma membrane (PM), early endosomes (EE), recycling endosomes (RE) and late endosomes/lysosomes (LE/Lys). Regulatory proteins and the transport steps they control, are indicated. (B) Bidirectional effect of transport from recycling endosomes on spine formation and loss. Forty-eight hours after transfection with the indicated constructs, neurons were fixed and imaged. Arrows indicate dendritic protrusions. Scale bar, 5 μ m. (C) Means \pm SEM of the number of protrusions per 10 μ m dendrite from (B). n = 36, 21, 28, 15, 18, 21, 18 for GFP, Rme1-WT, Rme1-G429R, Rab11a-WT, Rab11a-S25N, Syn13-WT, Syn13 Δ TM, **p < 0.05, *p < 0.001 relative to GFP; t test. (D and E) Acutely applied cell-permeable TAT-Syn13 Δ TM abruptly reduces the number of dendritic protrusions. Twenty-four hours after transfection with tdTomato at DIV17, neurons were imaged before and after applying Alx488-TAT-Syn13 Δ TM (3.5 μ M). Arrows mark the loss of dendritic protrusions over time. Scale bars, 3 μ m in (D) and 2 μ m in (E). (F and G) Change in total dendritic protrusion number following application of TAT fusion proteins. N values correspond to the total protrusion number at each time point. N₀ is the average number of dendritic protrusions before application of the indicated TAT fusion proteins. Data indicate means \pm SEM, n = 4 and 3 for (F) and (G), respectively.

amount of membrane added to each spine following glycine stimulation is similar. Interestingly, we observed a small but significant spine loss upon D-AP5 application in the absence of glycine stimulation (Figure 4C), indicating that maintenance of spines under basal conditions also required NMDA receptor activation. In our glycine-induced LTP protocol using 14–18 DIV cultured hippocampal neurons, glycine stimulation produced a 2.5-fold increase in the total number of protrusions (Figures 4C–4E) or an \sim 2-fold increase in the size of protrusions (Figures 4G–4I). Before glycine stimulation, neurons had 2.8 ± 0.8 protrusions per 10 μ m dendrite (n = 5). After glycine stimulation, the number of protrusions increased to 6.9 ± 1.6 protrusions per 10 μ m dendrite. These findings indicate that glycine stimulation induces spine plasticity similar to classically elicited

LTP in hippocampal slice preparations, providing an experimental system amenable to cell biological and biochemical studies of LTP-induced spine morphological plasticity.

Blocking Recycling Endosome Transport Prevents LTP-Induced Spine Growth

Based on our observation that promoting transport from recycling endosomes increased the number of spines (Figures 3B and 3C), as did LTP-inducing stimuli (Figure 4), we reasoned that LTP-associated spine growth could be occurring via accelerated membrane traffic from recycling endosomes. To test this possibility, we examined glycine-induced spine growth in neurons in which endocytic recycling was blocked by expression of Rme1-G429R or Rab11a-S25N. Unlike control

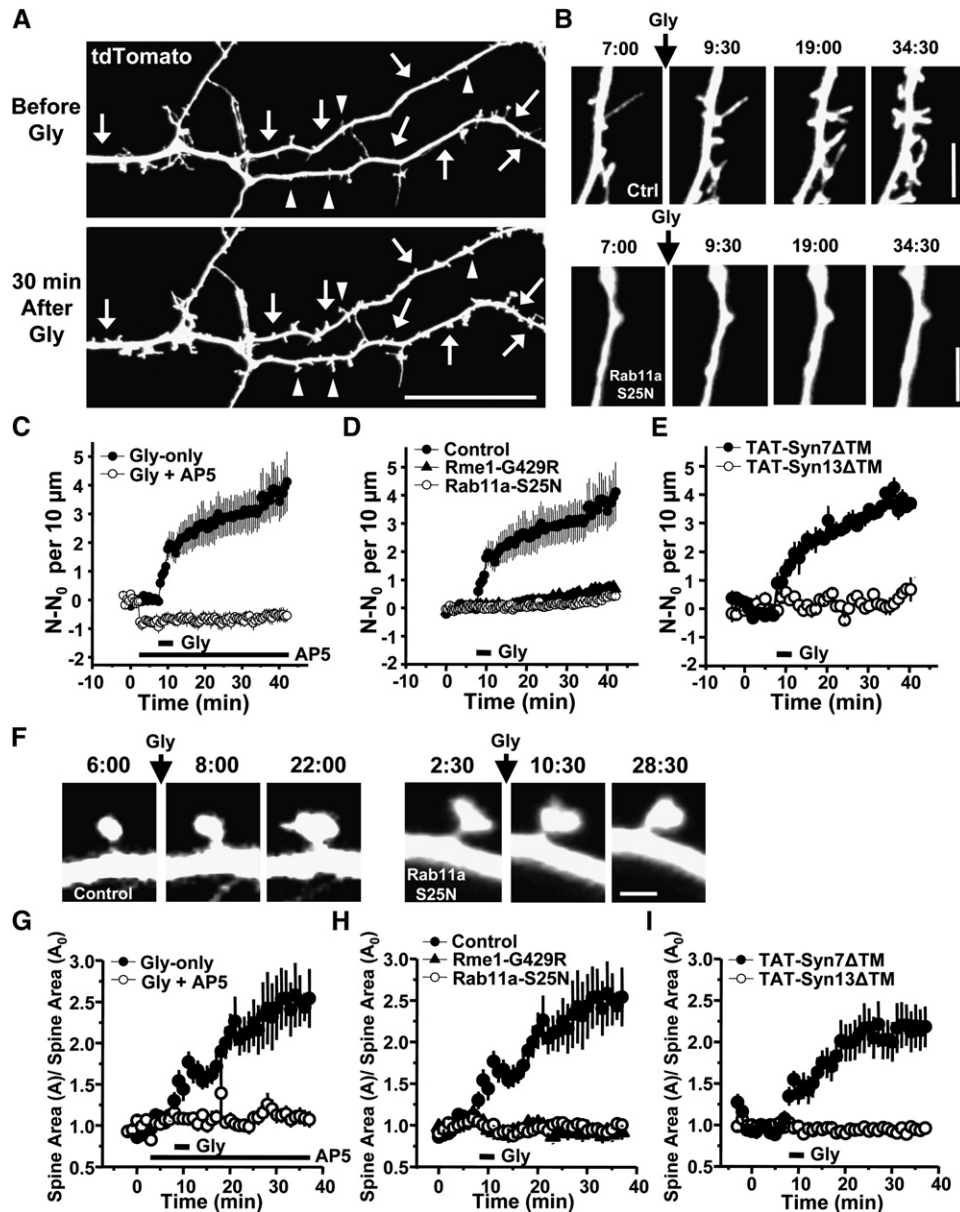


Figure 4. Blocking Recycling Endosome Transport Abolishes LTP-Induced New Spine Formation and Preexisting Spine Growth

(A) Glycine stimulation induces new spine formation (arrows) and preexisting spine growth (arrowheads). Neurons expressing tdTomato as a cell fill (DIV 14–18) were stimulated with glycine (200 μ M, 3 min), and then imaged for 30 min after glycine stimulation. Scale bar, 20 μ m.

(B) Formation and growth of dendritic protrusions following glycine stimulation (arrow) in neurons expressing tdTomato (top, Control) or GFP-Rab11a-S25N (bottom) to block recycling endosome transport. tdTomato is expressed as a cell fill. Times are indicated in min:sec. Scale bar, 3 μ m. See [Movie S1](#).

(C) Quantitative analysis of spine formation following glycine stimulation. N, number of dendritic protrusions per 10 μ m at the indicated time. N_0 , average number of dendritic protrusions per 10 μ m before application of glycine or AP5. Glycine (200 μ M) and D-AP5 (100 μ M) were applied at the times indicated by bars. $n = 5$ each. Data represent means \pm SEM.

(D) Glycine-stimulated spine formation is blocked by expression of Rme1-G429R or Rab11a-S25N. Twenty-four to 48 hr after transfection, neurons were imaged before and after glycine treatment. $n = 5$ each. Analysis as in (C).

(E) Acute application of Alexa 488-TAT-Syn13 Δ TM prevents LTP-induced formation of new dendritic protrusions. Neurons expressing tdTomato were preincubated with either Alexa-488-TAT-Syn13 Δ TM or Alexa-488-TAT-Syn7 Δ TM (3.5 μ M each) for 2 hr and imaged before and after glycine stimulation. $n = 6$ and 4 for TAT-Syn13 Δ TM and TAT-Syn7 Δ TM, respectively. Analysis as in (C).

(F) Growth of preexisting spines following glycine stimulation in neurons expressing tdTomato either alone (left panels, Control) or with GFP-Rab11a-S25N (right panels, Rab11a-S25N). Times are indicated in min:sec. Scale bar, 1 μ m. See [Movie S2](#).

(G) Quantitative analysis of spine growth following glycine stimulation. Spine area (A) indicates the spine area of the individual spine at the indicated time. A_0 indicates the average of spine areas before application of glycine or AP5. Glycine (200 μ M) and D-AP5 (100 μ M) were applied at the times indicated by bars. $n = 15$ spines on 3–4 neurons each. Data represent means \pm SEM.

(H) Glycine-stimulated preexisting spine growth is blocked by expression of Rme1-G429R or Rab11a-S25N. Experiments as in (D). $n = 15, 15, 14$ spines on 3–4 neurons each for Control, Rme1-G429R, Rab11a-S25N. Analysis as in (G).

(I) Acute application of Alexa 488-TAT-Syn13 Δ TM prevents LTP-induced growth of preexisting spines. Experiments as in (E). $n = 16$ and 10 spines on 2 neurons each for TAT-Syn13 Δ TM and TAT-Syn7 Δ TM, respectively. Analysis as in (G).

neurons, which displayed robust glycine-induced spine formation (Figures 4A–4C) and preexisting spine growth (Figures 4A, 4F, and 4G), neurons expressing Rme1-G429R or Rab11a-S25N failed to form new dendritic protrusions (lower panel, Figure 4B; Figure 4D; see also Movie S1) and exhibited no detectable spine growth (right panel, Figure 4F; Figure 4H; see also Movie S2) upon glycine stimulation. We have shown previously that blocking recycling endosome transport does not affect immunocytochemically detected NMDA receptors at synapses or NMDA receptor-mediated synaptic currents (Park et al., 2004). In addition, postsynaptic expression of Rme1-G429R, Rab11a-S25N, or Syn13 Δ TM had no effect on FM4-64 uptake into contacting presynaptic terminals (Figure S5) and no effect on the magnitude or kinetics of evoked NMDA receptor currents in cultured hippocampal neurons (Figure S6), indicating that expressing neurons had functional synapses with unchanged synaptic NMDA receptor currents. Thus, the observed inhibition of spine growth during glycine-induced LTP cannot be accounted for by a decrease of functional NMDA receptors or altered presynaptic function.

To rule out effects of chronic disruption of endocytic recycling, neurons were pretreated with cell-permeable TAT-Syn13 Δ TM (3.5 μ M) for 2 hr prior to time-lapse imaging to acutely block recycling transport. Following incubation with TAT-Syn13 Δ TM, neurons showed no increase in spine number (Figure 4E) or spine size (Figure 4I) following glycine stimuli. In contrast, TAT-Syn7 Δ TM-pretreated neurons exhibited a robust increase in spine number (Figure 4E) and spine size (Figure 4I) upon glycine stimulation. Short-term incubation with TAT-Syn13 Δ TM (3.5 μ M, 2 hr, 37°C) had no effect on FM4-64 uptake or destaining kinetics (Figure S7), indicating that the effect of TAT-Syn13 Δ TM was not due to altered presynaptic function. Taken together, these results indicate that recycling endosomes supply membrane or molecular material for the formation and growth of spines during LTP.

Recycling Endosomes Translocate into Spines following LTP Stimuli

Under nonstimulating conditions, many spines lack recycling endosomes, which instead reside at the base of spines in the dendritic shaft (Figures 1C and 1E). To test whether recycling endosomes move into spines following LTP stimuli, we analyzed the localization of recycling endosomes before and after glycine stimulation. In these experiments, recycling endosomes were visualized by expressing GFP-tagged transferrin receptor (TfR-GFP), a classic recycling cargo which at steady state resides in recycling endosomes (Lin et al., 2001). In hippocampal neuron dendrites, exogenously expressed TfR-GFP colocalized with internalized Alexa-Tf (60 min, 37°C), which functionally labels the endocytic recycling pathway but not the classical secretory pathway (Figure 5A). In the absence of stimulation, the distribution of TfR-GFP was identical to that of Alexa-Tf, with TfR-GFP-labeled endosomes present in a small proportion of spine heads but frequently present in the dendritic shaft at the base of spines (Figures 5B and 5C). Shortly after activation of synaptic NMDA receptors to elicit chemical LTP (200 μ M glycine, 3 min), TfR-

GFP-labeled endosomes coalesced into more compact structures that extended into the spine neck and were much more abundant in the spine head itself (Figure 5B). Quantitative analysis revealed that 82% of spines had recycling endosomes at their base before glycine stimulation (a, Figure 5C). In addition, a subpopulation of spines had TfR-GFP endosomes in their neck (22%; b, Figure 5C), in the spine head proper (26%; c, Figure 5C), throughout the base and neck (6%; a + b, Figure 5C), or throughout the head and neck (2%; b + c, Figure 5C). This distribution pattern of TfR-GFP was similar to that of observed by labeling recycling endosomes with Alexa-Tf, TfR, and Rab11 (Figure 1C). Twenty minutes after glycine stimulation, however, only 30% of spines had recycling endosomes situated exclusively at their base in the dendritic shaft (a, Figure 5C). Instead, recycling endosomes were much more abundant in the spine head (52% of spines; c, Figure 5C), throughout the base and neck of spines (42%; a + b, Figure 5C), throughout the neck and head of spines (6%; b + c, Figure 5C), or throughout the base, neck, and head of spines (8%; a + b + c, Figure 5C). Thus, the distribution of recycling endosomal compartments shifts from the dendritic shaft near the base of spines into the spine proper following glycine stimulation, supporting a direct physical movement of endosomes into spines upon LTP stimuli.

To more directly visualize the movement of endosomes during LTP, we performed time-lapse imaging of hippocampal neurons coexpressing TfR-GFP and mRFP. Under basal conditions, TfR-GFP labeled large endosomes and mobile endocytic vesicles throughout dendrites. Elongated endosomes were frequently present at the base of dendritic spines, where they exhibited small lateral movements but remained apposed to the emergence point of the spine neck (Figure 5D, left panels; Movies S3A and S3B). Occasional vesicles or tubules were observed to bud from spine base-associated endosomes and move into the spine (Figure 5Db, panel second from left; Movie S3B). Within minutes after glycine stimulation, individual endosomes became more compact near the base of the spine and extruded into the spine neck (Figure 5D, middle panels; Movies S3A and S3B). Following intrusion into the spine, discrete endosomal extensions, tubules, and vesicles could be seen budding from the endosome and moving outward toward the spine plasma membrane (Figure 5D, right panels; Movies S3A and S3B). Quantitative line-scan analysis through the dendrite and spine showed that TfR-GFP fluorescence that was initially concentrated in the dendritic shaft moved rapidly and progressively into spines following glycine-LTP (Figure 5E). In addition, a comparison of fluorescence intensity of TfR-GFP in spines with that in adjacent regions of the dendritic shaft revealed an abrupt increase of TfR-GFP in the spine following glycine stimulation that was coincident with a corresponding decrease in TfR-GFP fluorescence in the apposing segment of the dendritic shaft (Figure 5F). Notably, the absolute increase in spine TfR-GFP fluorescence was very similar to the absolute decrease in shaft fluorescence (Figure 5F), consistent with direct local endosome translocation rather than accumulation of TfR-GFP from a more distant source. The movement of TfR-GFP-positive endosomes into spines occurred over several minutes and persisted for the

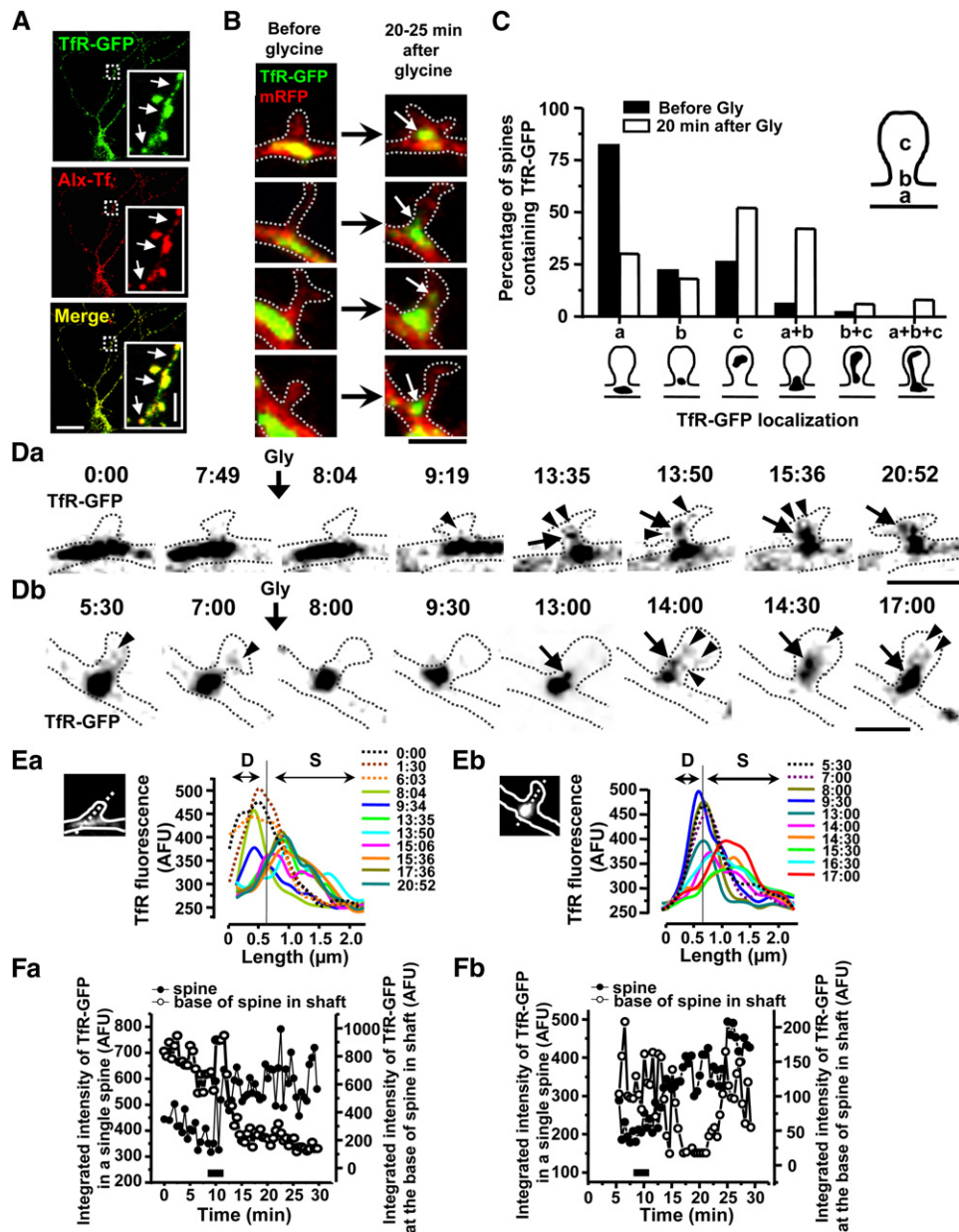


Figure 5. Recycling Endosomes Move into Spines in Response to LTP-Inducing Stimuli

(A) TfR-GFP labels recycling endosomes in hippocampal neurons. Alexa-transferrin (Alexa-Tf) was applied to live neurons expressing TfR-GFP for 1 hr at 37°C to functionally label recycling endosomes. Neurons were fixed and imaged. Arrows indicate the colocalization of TfR-GFP and Alexa-Tf. Scale bars, 20 μ m in the large panels and 3 μ m in the insets.

(B) Neurons were cotransfected with TfR-GFP to label recycling endosomes and mRFP as a cell fill. Before glycine stimulation, recycling endosomes (TfR-GFP) are present in the dendritic shaft at the base of spines (left panels). Following glycine stimulation, recycling endosomes coalesce in the spine neck and physically extrude into spines (right panels). Scale bar, 2 μ m.

(C) Proportion of spines containing TfR-GFP positive endosomes at the indicated locations. n = 50 spines from 3 neurons.

(D) Time lapse imaging of recycling endosomes mobilized into spines following glycine stimulation. Neurons expressing TfR-GFP and mRFP were imaged every 15–30 s before and after glycine stimulation (200 μ M, 3 min). Two examples are shown (Da and Db). Times are indicated in min:sec. Arrows indicate the movement of large endosomes into the spine from the shaft. Arrowheads indicate vesicles or tubules emanating from larger TfR-containing endosomes. Scale bars, 2 μ m in (Da), 1 μ m in (Db). See [Movies S3A](#) and [S3B](#).

(E) Line-scan analysis of TfR-GFP fluorescence through individual dendritic spines and the corresponding apposed segment of the dendritic shaft. Two examples are shown (Ea and Eb). TfR-GFP fluorescence intensity along the white dotted lines in inset images is plotted at various times before (dotted lines) and after (solid lines) glycine stimulation. D and S indicate dendrite and spine, respectively. Times are indicated in min:sec.

(F) Integrated intensity of TfR-GFP fluorescence was measured both in individual spines (black circles) and at the base of spine in the shaft (open circles) over time. Two examples are shown (Fa and Fb). The black bar indicates the duration of glycine application. The increase of TfR-GFP in spines occurs simultaneous with the decrease in the adjacent dendritic shaft.

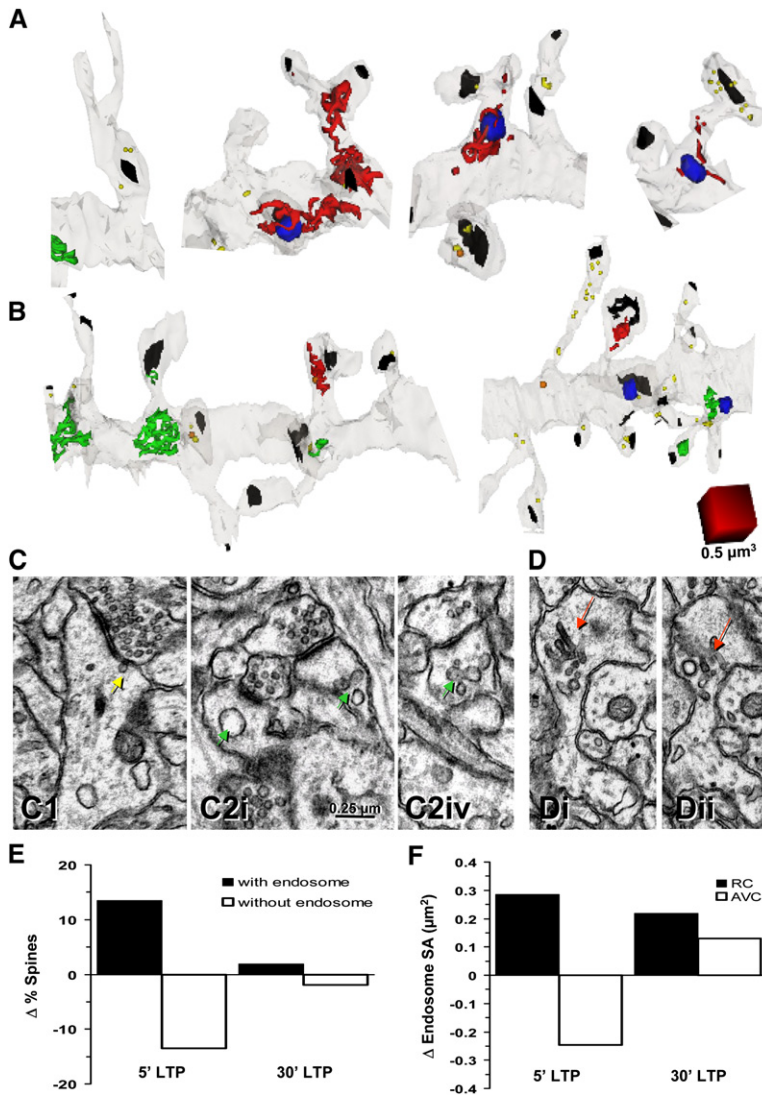


Figure 6. Plasticity of Endosomes in Spines during LTP in Hippocampal Slices

(A and B) Dendritic segments at 5 min (A) and 30 min (B) after LTP induction by theta-burst stimulation (TBS). Endosomal compartments including recycling compartments (RCs, red), amorphous vesicular clumps (AVCs, green), multivesicular bodies (MVBs, blue), and free endosomes (yellow or orange) are illustrated. Synapses are marked with black. Scale cube, $0.5 \mu\text{m}^3$.

(C and D) Electron micrographs from dendritic segments at 5 min (C) and 30 min (D) after LTP induction. A smooth vesicle (yellow arrow) apparently inserting at a spine head (C1), a large vesicle in the left spine head ([C2i], left green arrow), and an AVC in the right spine head from the same dendrite ([C2i], right green arrow) are shown. Four serial sections later (C2iv), the AVC is still present in the spine head (green arrow). Adjacent serial sections (Di and Dii) show a RC with multiple tubules and vesicles (red arrows) in a large spine head. Scale bar in (C2i) is for all images in (C) and (D).

(E) Spines contain more endosomes within minutes after TBS. The graph shows relative change in the percentage of spines with or without endosomes at 5 and 30 min after TBS.

(F) Quantitative analysis of endosome area in spines following LTP. The graph shows changes in the surface area (SA) of RCs and AVCs at 5 and 30 min after TBS. Values in (E) and (F) are relative to average values of all control spines. $n = 14$ dendritic segments each whose average length was $8.5 \mu\text{m}$ for control and $8.0 \mu\text{m}$ for LTP; a total of 199, 89, and 91 dendritic spines were analyzed in the control, in the 5 min LTP condition, and in the 30 min LTP condition, respectively. See [Experimental Procedures](#) for details.

20–30 min duration of the imaging experiments. Taken together, these findings demonstrate that recycling endosomes are mobilized into spines upon LTP-inducing stimuli where they engage in active local membrane trafficking.

Plasticity of Endosomal Compartments following LTP in Acute Hippocampal Slices

We next examined whether LTP in hippocampal slice preparations also redistributes endosomes into the spines. For this, we performed 3D reconstructions from sSTEM on dendritic segments in hippocampal slices (PN15) that had been subjected to control stimulation or repeated theta-burst stimulation (TBS; see [Experimental Procedures](#) for details) to induce LTP.

Five minutes after LTP induction (Figures 6A and 6C), the percentage of spines containing RCs or AVCs was increased (+13.5% increase relative to control; 5 min LTP; Figure 6E), consistent with the recruitment of recycling endosomes into spines (Figure 5). By 30 min after LTP induction (Figures 6B and 6D), the relative frequencies of spines harboring endosomal compartments returned nearly to control levels (+1.9% relative to control;

30 min LTP; Figure 6E). These findings suggest that recycling endosomes that had moved into spines within 5 min either exited spines or were rapidly depleted by local exocytosis to the spine membrane. Supporting the latter, average spine surface area increased following TBS ($+0.22 \mu\text{m}^2$, 5 min LTP) relative to control stimulation (data not plotted). Quantitative analysis revealed a sustained increase in the membrane surface area of recycling compartments (RCs) after TBS ($+0.29 \mu\text{m}^2$ at 5 min relative to control stimulation; $+0.22 \mu\text{m}^2$ at 30 min; Figure 6F), consistent with the mobilization of recycling endosomes into spines (Figure 5). Intriguingly, the membrane surface area of individual AVCs was reduced by $-0.25 \mu\text{m}^2$ at 5 min after TBS (Figure 6F). This decrease in AVC membrane area was nearly identical with the measured increase in spine surface area ($+0.22 \mu\text{m}^2$), supporting a direct transfer of membrane, and suggesting that AVCs present in spines may undergo rapid fusion with the spine membrane following LTP stimulation. By 30 min after TBS, AVCs were replenished to $+0.13 \mu\text{m}^2$ above control levels (Figure 6F). These findings suggest that AVCs are a proximal source of exocytic material for rapid spine growth. Furthermore,

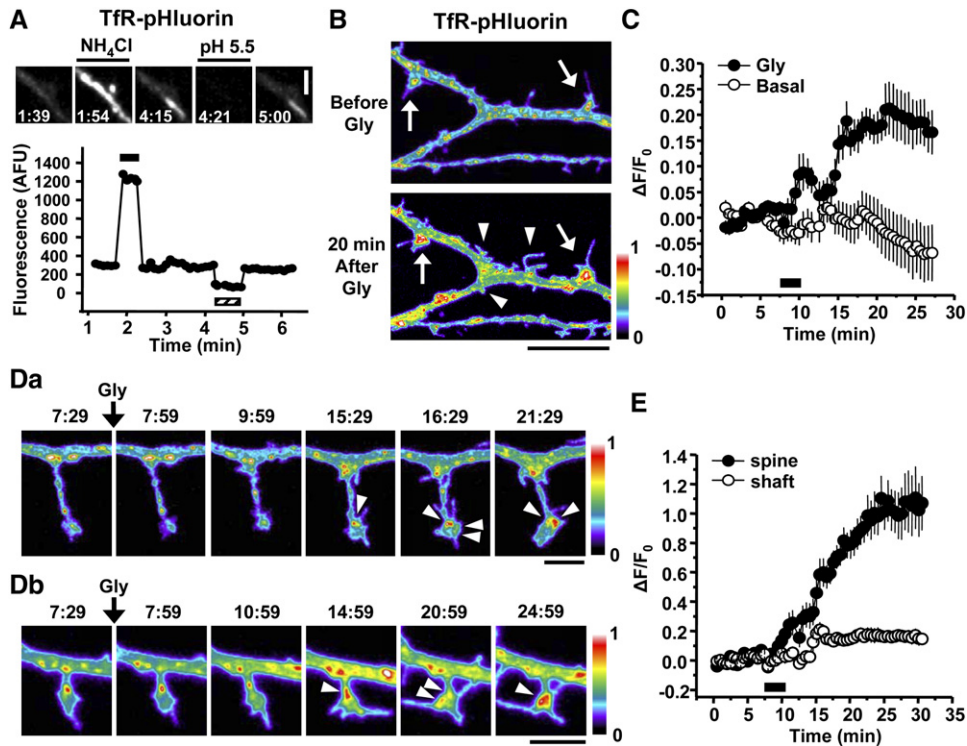


Figure 7. Exocytosis from Recycling Endosomes on Dendrites and Spines following LTP

(A) Visualization of externalized recycling cargo using transferrin receptor-superecliptic pHluorin (Tfr-pHluorin). Fluorescence signal from lumenally tagged Tfr-pHluorin in a stretch of dendrite was monitored during brief exposures to alkaline solution (NH_4Cl , black bar in lower panel) and to acidic solution (pH 5.5, hatched bar in lower panel). The graph shows a quantitative analysis of fluorescence intensity. Times in the images are indicated in min:sec. Scale bar, $3 \mu\text{m}$.

(B) Exocytosis of Tfr-pHluorin following glycine-induced LTP. Tfr-pHluorin fluorescence was imaged before (top) or 20 min after (bottom) glycine stimulation. Arrows and arrowheads indicate growing and newly formed dendritic protrusions, respectively. A pseudocolor intensity scale bar is shown. Scale bar, $10 \mu\text{m}$. See *Movie S4*.

(C) Quantitative analysis of surface appearing Tfr-pHluorin over hippocampal neuron dendrites. Data represent means \pm SEM of the change in fluorescence intensity (ΔF) normalized to the average of initial fluorescence intensity prior to glycine stimulation (F_0). The black bar indicates the period of glycine application. $n = 12$ dendritic segments from 6 neurons ($1090 \mu\text{m}$ in dendritic length analyzed) and 10 dendritic segments from 3 neurons ($894 \mu\text{m}$ in dendritic length analyzed) for Gly and Basal, respectively.

(D) Local exocytosis from recycling endosomes in spines. Tfr-pHluorin was imaged before and after glycine stimulation as indicated in the two examples (Da and Db). Note the appearance of externalized Tfr-pHluorin within the spine head (arrowheads). Times in the images are indicated in min:sec. Pseudocolor intensity scale bars are shown. Scale bars, $3 \mu\text{m}$ each. See *Movie S5*. For more examples, see *Movie S6*.

(E) Data represent means \pm SEM of $\Delta F/F_0$ from spines (dark circles; $n = 15$) and segments of the dendritic shaft (open circles; $n = 12$). The black bar indicates the period of glycine application. Note the ordinate scale difference compared to (C).

the increase in the membrane surface area of both RCs and AVCs at 30 min after TBS suggests that recycling endosomal compartments sustain localized endosomal transport in potentiated spines.

LTP Stimuli Trigger Local Exocytosis from Recycling Endosomes

Detection of exocytotic events in spines has been elusive. To directly visualize membrane delivery from recycling endosomes, we took advantage of a pH-sensitive variant of GFP (superecliptic pHluorin) whose fluorescence is quenched at low pH by fusing superecliptic pHluorin to the luminal domain of the Tfr (Tfr-pHluorin) (Merrifield et al., 2005). At steady state, most Tfr-pHluorin is present in endosomal compartments whose acidic lumen quenches pHluorin fluorescence, allowing for surface Tfr-pHluorin to be selectively visualized (Merrifield et al., 2005). Correspondingly, expression of Tfr-pHluorin in hippocampal neurons showed only a dim surface signal over individual dendrites (Figure 7A,

left panel). Application of NH_4Cl to alkalinize intracellular compartments resulted in an immediate increase in Tfr-pHluorin fluorescence (Figure 7A) and this effect was rapidly reversible (Figure 7A). Conversely, application of acidic solution (pH 5.5) completely and rapidly quenched Tfr-pHluorin fluorescence and this effect was also rapidly reversible (Figure 7A). Thus, Tfr-pHluorin provides a powerful tool for studying exocytosis from recycling endosomes.

To test whether LTP stimuli trigger exocytosis from recycling endosomes, we monitored Tfr-pHluorin fluorescence over hippocampal neuron dendrites following glycine stimulation. Before glycine stimulation, discrete spots of Tfr-pHluorin signal were observed (Figure 7B, top panel), suggesting ongoing spatially restricted endocytic recycling and dendritic exocytosis. The observed Tfr-pHluorin signal was completely quenched by pH 5.5 solution (Figure 7A and data not shown) supporting the presence of a proportion of the Tfr-pHluorin reporter at the cell surface. Soon after glycine

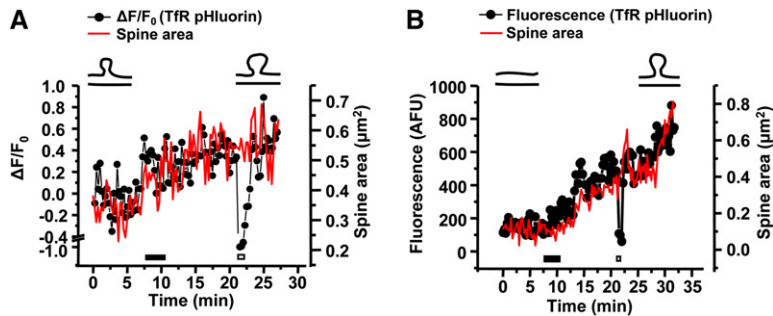


Figure 8. LTP-Induced Spine Growth Is Simultaneous with Exocytosis from Recycling Endosomes

(A and B) Quantitative changes in spine area (red line) and TfR-pHluorin fluorescence (black line) over time following glycine stimulation (black bar) during growth of existing spines (A) or new spine formation (B). The empty bar indicates application of pH 5.5 solution.

stimulation, TfR-pHluorin fluorescence was significantly increased over the dendrite, including notable exocytosis on dendritic spines (Figures 7B and 7C; see also Movie S4). Close examination of spines revealed robust exocytosis from recycling endosomes directly on the spine head (Figure 7D). We frequently observed hot spots of TfR-pHluorin fluorescence that appeared suddenly on spines, often at lateral domains, which then dispersed laterally in the spine membrane (see Movies S5 and S6). Spines displayed $\Delta F/F_0$ values that were 5- to 6-fold higher than that observed in the dendritic shaft (Figure 7E; note the ordinate scale difference between Figures 7C and 7E). Additional exocytosis from recycling endosomes was also evident at the base of spines and in the dendritic shaft (Figures 7B and 7D). Intriguingly, $\Delta F/F_0$ values of TfR-pHluorin in segments of the dendritic shaft near spines were 2- to 4-fold higher than those observed in shaft segments away from spines (Figure S8). Although the absolute amount of shaft exocytosis was much less than that observed in the spine head proper, these findings nonetheless indicate the presence of both intraspinous and perispinous pathways of stimulus-dependent exocytosis from recycling endosomes. Unlike the growth of spines triggered by LTP stimuli (Figure 4G), we detected no increase in the size of dendritic shafts upon glycine stimulation (Figure S9). Taken together, these data show that LTP stimuli trigger exocytosis from recycling endosomes and that this exocytosis occurs preferentially, but not exclusively, at the spine membrane.

Spine Enlargement Accompanies Exocytosis from Recycling Endosomes

To define the relationship between spine growth and exocytosis, we simultaneously monitored spine size and surface appearance of TfR-pHluorin over individual spines. Hippocampal neurons were cotransfected with TfR-pHluorin and mRFP as a cell fill. TfR-pHluorin fluorescence intensity and spine area were monitored on both preexisting (Figure 8A) and newly formed spines (Figure 8B) before and at various times after glycine stimulation. As above (Figure 7), glycine stimulation triggered a progressive increase in TfR-pHluorin fluorescence on spines corresponding to externalized TfR-pHluorin (Figures 8A and 8B). This increase in exocytosed TfR-pHluorin occurred in precise temporal register with a progressive increase in spine size (Figure 8A) and with the emergence of a new dendritic protrusion (Figure 8B). Interlaced exposure to acidic solution (pH 5.5) revealed a selective loss of TfR-pHluorin fluorescence, indicating that the increase in TfR-pHluorin fluorescence was due to newly

exocytosed recycling endosome cargo. Together, these results demonstrate that spine growth accompanies localized exocytosis from recycling endosomes, supporting a role for membrane delivery from recycling endosomes in spine morphological plasticity.

Discussion

In the present study, we have demonstrated that LTP triggers dendritic spine formation and growth through an unanticipated mechanism involving relocalization of and enhanced exocytotic trafficking from recycling endosomes. In the absence of a plasticity stimulus, recycling endosomes and endosomal vesicles stably localize to the base of spines, and ongoing transport from recycling endosomes maintains the spine membrane. Activation of synaptic NMDA receptors to elicit LTP causes rapid mobilization of recycling endosomes and endosomal vesicles into spines and triggers local exocytosis from recycling endosomes. The emergence of new spines and growth of existing spines occurs concurrently with exocytosis from recycling endosomes. In the absence of recycling endosome transport, spines are rapidly lost, and LTP stimuli fail to elicit spine growth (Figure 9).

Recycling Endosomes as Multipurpose Organelles for Synapse Plasticity

NMDA receptor-dependent transport from recycling endosomes may provide a unifying cellular mechanism linking functional and structural plasticity at glutamatergic synapses. Work from several laboratories has established that LTP-inducing stimuli promote the physical insertion of AMPA receptors at the postsynaptic membrane, leading to an increase in AMPA receptor-mediated transmission at excitatory synapses (Malenka and Nicoll, 1999). In addition to functional enhancement, LTP-inducing stimuli cause the formation and enlargement of dendritic spines (Engert and Bonhoeffer, 1999; Matsuzaki et al., 2004), a structural remodeling of synapses thought to consolidate neural circuitry. Intriguingly, the very same stimuli and signaling pathways—NMDA receptor activation, calcium influx, CaMKII activation—that mediate synaptic potentiation produce spine structural changes, suggesting a common mechanistic link that has been elusive. We have previously shown that recycling endosomes supply AMPA receptors for LTP (Park et al., 2004). Here we have shown that, in addition to supplying AMPA receptors and thereby effecting potentiation of excitatory synaptic transmission, membrane trafficking from recycling endosomes mediates the structural

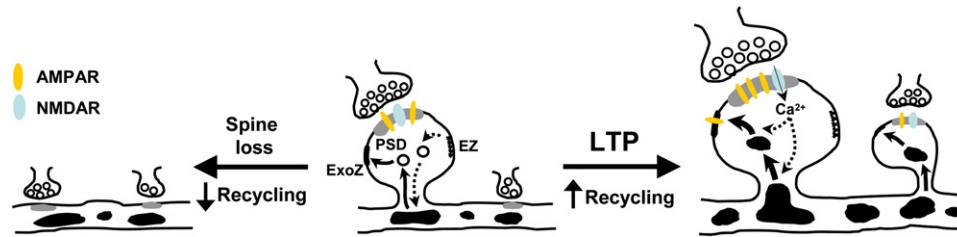


Figure 9. Schematic Model for Recycling Endosome Transport in Spine Morphological Plasticity

Intracellular organelles filled in black are recycling endosomes. PSD, postsynaptic density; ExoZ, exocytic zone; EZ, endocytic zone. See text for details.

growth and expansion of dendritic spines during LTP. Following an LTP stimulus, recycling endosomes physically translocate into spines, and exocytosis of membrane cargo from endosomes is increased. Such intimately coupled AMPA receptor insertion and membrane addition from recycling endosomes may help explain the tightly correlated scaling of spine size with AMPA receptor-mediated synaptic currents (Matsuzaki et al., 2001) and could plausibly account for the precise temporal relationship between spine enlargement and potentiation of AMPA receptor-mediated currents following single synapse LTP (Matsuzaki et al., 2004).

Our results further suggest that mechanisms linking LTP induction and expression may converge on the recycling endosome. Several effectors of endosomal transport and vesicular fusion are Ca^{2+} sensitive (Khvotchev et al., 2003) or targets of CaMKII (Karcher et al., 2001), the central intracellular signals for LTP. Furthermore, endosomal transport and activity-induced insertion of AMPA receptors are regulated by cAMP-dependent protein kinase (PKA) (Ehlers, 2000), a well-known signaling molecule for LTP. Indeed, many of the diverse signaling mechanisms shown to affect LTP either occur on endosomes or influence endosomal trafficking (Steiner et al., 2002; Bivona and Philips, 2003). It is therefore tempting to speculate that recycling endosomes may function as central integrators and cellular effectors for LTP expression. Interestingly, at the *Drosophila* neuromuscular synapse, synaptotagmin-4 serves as a postsynaptic Ca^{2+} sensor that retrogradely regulates presynaptic neurotransmitter release, likely by regulated exocytosis of postsynaptic cargos (Yoshihara et al., 2005), emphasizing an emerging and evolutionarily conserved role for regulated postsynaptic vesicular trafficking. Clearly, it will be important for future studies to delineate the protein machinery on endosomes that senses and responds to NMDA receptor-mediated Ca^{2+} influx during LTP.

Membranes for Spine Morphological Plasticity

To date, mechanisms for spine morphological plasticity have centered on the actin cytoskeleton (Fischer et al., 1998; Okamoto et al., 2004; Terry-Lorenzo et al., 2005; Tada and Sheng, 2006). Actin reorganization in spines is highly dynamic and responsive to synaptic signals (Okamoto et al., 2004). Along with reorganization of the actin cytoskeleton, it is apparent that spine growth and new spine formation require additional membrane. Yet, despite extensive dissection of cytoskeletal regula-

tion, it has been unclear how and from where membrane material is provided during spine remodeling.

Results presented here support a direct link between recycling endosome transport and spine structural plasticity. In particular, our findings indicate that activation of synaptic NMDA receptors triggers translocation and exocytosis of recycling endosomes to mediate spine growth. Such exocytic membrane trafficking is likely coordinated with actin reorganization to effect spine structural plasticity. Although the molecular mechanisms coordinating spine actin remodeling and membrane trafficking are as yet unclear, it is interesting to note that actin-based myosin motors and myosin regulatory proteins are abundant in dendritic spines and influence spine structure (Osterweil et al., 2005; Ryu et al., 2006).

The growth and formation of dendritic spines by exocytic trafficking from recycling endosomes could occur by the simple addition of lipid membrane, by the delivery of membrane proteins and secreted molecules that regulate spine morphogenesis, or by a combination of both. Using high-resolution electron microscopic reconstruction, we have shown that intradendritic endosomal membranes near spines have ample surface area to account for expansion of the spine plasma membrane during LTP, including the de novo formation of new small spines. Yet, it is likely that, in addition to AMPA receptors (Park et al., 2004) and lipid membrane, additional membrane proteins delivered to the spine membrane from recycling endosomes alter the adhesive or signaling properties of spines which either promote spine growth or stabilize spine structure. Dissecting the compositional changes in spines mediated by LTP-induced endosomal recycling is a fertile topic for future investigation.

Establishment and Regulation of a Local Endosomal Cycling System in Spines

Regulated membrane trafficking of postsynaptic neurotransmitter receptors has emerged as a central mechanism for synapse development and modification. The cellular machinery for highly compartmentalized trafficking in dendritic spines is only now beginning to be revealed. Much of what we know regarding spine composition and molecular organization comes from our detailed understanding of the PSD (Kennedy et al., 2005). Although a central element in spine organization and postsynaptic protein trafficking, the PSD occupies only 10%–15% of the spine membrane (Lisman and Harris, 1993), leaving open the question of how molecular components are delivered to and from the postsynaptic membrane. Recently, a lateral membrane domain

specialized for clathrin-mediated endocytosis in spines has been described (Blanpied et al., 2002; Racz et al., 2004), providing a platform for protein removal from the spine membrane that may be regulated by synaptic activity and intracellular signaling (Brown et al., 2005). The possibility that localized stimulus-dependent exocytosis occurs in spines has long been postulated (Lledo et al., 1998; Maletic-Savatic and Malinow, 1998), but has remained an open question, as has the identity of relevant intracellular membrane compartments.

Here we have shown that the entire apparatus for endosomal recycling can localize to spines, suggesting tight spatial control. The presence of recycling endosomes in spines along with the presence of endocytic zones on the spine plasma membrane (Blanpied et al., 2002; Racz et al., 2004) suggest that localized recycling transport plays a role in spine stabilization and maintenance. Indeed, spines containing endosomes are larger than spines lacking endosomes, and acute disruption of recycling transport by TAT-Syn13 Δ TM caused abrupt spine loss, supporting this notion that ongoing endocytic recycling maintains or stabilizes spines. Intriguingly, the establishment of this local endocytic recycling system is activity dependent in that LTP-inducing stimuli promote the physical translocation of recycling endosomes into spines. One consequence of such organelle movement would be to “focus” or restrict the membrane domain over which endocytic recycling can occur, effectively allowing for both local and dynamic regulation of membrane composition on a spine-by-spine basis. Consistent with this notion, we have shown that exocytosis from recycling endosomes occurs directly at the spine membrane. We suggest that exocytosis of recycling vesicles at “exocytic zones” of the spine delivers cargo which can then be repositioned via lateral diffusion over short distances to the PSD (Triller and Choquet, 2005). Such tight spatial and temporal control over endocytic cycling may allow for rapid “online” control over the number of postsynaptic AMPA receptors (Luscher et al., 1999; Ehlers, 2000). Patterns of synaptic activity may thus control AMPA receptor abundance and spine morphology by tuning the kinetics of endocytosis and recycling locally within spines. More broadly, such a mechanism may provide a general paradigm for localized regulation of cell morphology on a micron scale.

Experimental Procedures

DNA constructs, cell culture, immunocytochemistry, cargo uptake and recycling assays, purification and labeling of TAT fusion proteins, FM dye uptake and destaining, and electrophysiology methods are included in the [Supplemental Data](#).

Live-Cell Imaging

Twenty-four to 48 hr following transfection, neurons were imaged in a chamber (Dagan) filled with imaging buffer (pH 7.4). Confocal images were acquired using a Yokogawa spinning disk confocal (CSU10, Solamere Technology Group), a 60 \times Plan APOchromat objective (NA 1.4), and a 12-bit cooled CCD camera (Roper Scientific or Hamamatsu Inc.). For glycine stimulation, neurons were treated with glycine (200 μ M) in Mg²⁺-free extracellular solution for 3 min. For TIR-pHluorin imaging, acidic solution (pH 5.5) was prepared by replacing HEPES in the imaging buffer with MES. Ammonium chloride solution (pH 7.4) was prepared by substituting 50 mM NaCl in the imaging buffer with NH₄Cl. For other detailed methods, see [Supplemental Data](#).

Image Analysis and Quantification

Either mRFP or tdTomato channels of each image were scaled equally for counting spines and filopodia. The change in the total protrusion number was calculated by $N - N_0$. N corresponds to the total protrusion number at each time point, and N_0 indicates the average number of protrusions before application of glycine, AP5, Alexa-488-TAT-Syn13 Δ TM, or Alexa-488-TAT-Syn7 Δ TM as indicated. For measurements of TIR-pHluorin fluorescence during LTP, the change in fluorescence (ΔF) was normalized to the averaged fluorescence intensity (F_0) before glycine treatment. ΔF was calculated by subtraction of F_0 from the measured fluorescence intensity at each time point. More detailed descriptions of image analysis and quantification are available in the [Supplemental Data](#).

Serial Section Transmission Electron Microscopy

Hippocampal slices from PN15 animals were fixed at 5 min ($n = 2$ slices) or 30 min ($n = 3$ slices) after the delivery of TBS. Fixed slices were processed, sectioned, and analyzed as described in the [Supplemental Data](#). Serial section images were aligned using the Reconstruct software developed in the Harris laboratory (by John Fiala, available at <http://synapses.bu.edu>).

Immunogold Electron Microscopy

Immunogold labeling of adult rat CA1 hippocampus was performed with anti-TfR antibody (Zymed Laboratories Inc.) essentially as described (Horton et al., 2005). Further methods are provided in the [Supplemental Data](#).

Supplemental Data

The Supplemental Data for this article can be found online at <http://www.neuron.org/cgi/content/full/52/5/817/DC1/>.

Acknowledgments

We thank Marguerita Klein, Irina Lebedeva, Elizabeth Perry, Robert Smith, and Haiwei Zhang for excellent technical assistance. We thank Richard Weinberg for advice and assistance on immunogold electron microscopy. We thank Benjamin Arenkiel, Daniel Choquet, Kathryn Condon, Ian Davison, Laurent Groc, Martin Heine, Juliet Hernandez, Matthew Kennedy, Richard Mooney, Kanghyun Ryo, Ryohei Yasuda, and Jason Yi for critical review of the manuscript. This work was supported by grants MH064748, AG024492, NS047574, the American Health Assistance Foundation, and the Raymond and Beverly Sackler Foundation (to M.D.E.) and grants NS33574, NS21184, and EB002170 (to K.M.H.). M.D.E. is an Investigator of the Howard Hughes Medical Institute.

Received: May 30, 2006

Revised: September 14, 2006

Accepted: September 27, 2006

Published: December 6, 2006

References

- Bivona, T.G., and Philips, M.R. (2003). Ras pathway signaling on endomembranes. *Curr. Opin. Cell Biol.* 15, 136–142.
- Blanpied, T.A., Scott, D.B., and Ehlers, M.D. (2002). Dynamics and regulation of clathrin coats at specialized endocytic zones of dendrites and spines. *Neuron* 36, 435–449.
- Brown, T.C., Tran, I.C., Backos, D.S., and Esteban, J.A. (2005). NMDA receptor-dependent activation of the small GTPase Rab5 drives the removal of synaptic AMPA receptors during hippocampal LTD. *Neuron* 45, 81–94.
- Calabrese, B., and Halpain, S. (2005). Essential role for the PKC target MARCKS in maintaining dendritic spine morphology. *Neuron* 48, 77–90.
- Cooney, J.R., Hurlburt, J.L., Selig, D.K., Harris, K.M., and Fiala, J.C. (2002). Endosomal compartments serve multiple hippocampal dendritic spines from a widespread rather than a local store of recycling membrane. *J. Neurosci.* 22, 2215–2224.
- Ehlers, M.D. (2000). Reinsertion or degradation of AMPA receptors determined by activity-dependent endocytic sorting. *Neuron* 28, 511–525.

- Engert, F., and Bonhoeffer, T. (1999). Dendritic spine changes associated with hippocampal long-term synaptic plasticity. *Nature* 399, 66–70.
- Fischer, M., Kaech, S., Knutti, D., and Matus, A. (1998). Rapid actin-based plasticity in dendritic spines. *Neuron* 20, 847–854.
- Grutzendler, J., Kasthuri, N., and Gan, W.B. (2002). Long-term dendritic spine stability in the adult cortex. *Nature* 420, 812–816.
- Hering, H., and Sheng, M. (2001). Dendritic spines: structure, dynamics and regulation. *Nat. Rev. Neurosci.* 2, 880–888.
- Hopkins, C.R., Gibson, A., Shipman, M., Strickland, D.K., and Trowbridge, I.S. (1994). In migrating fibroblasts, recycling receptors are concentrated in narrow tubules in the pericentriolar area, and then routed to the plasma membrane of the leading lamella. *J. Cell Biol.* 125, 1265–1274.
- Horton, A.C., Racz, B., Monson, E.E., Lin, A.L., Weinberg, R.J., and Ehlers, M.D. (2005). Polarized secretory trafficking directs cargo for asymmetric dendrite growth and morphogenesis. *Neuron* 48, 757–771.
- Karcher, R.L., Roland, J.T., Zappacosta, F., Huddleston, M.J., Annan, R.S., Carr, S.A., and Gelfand, V.I. (2001). Cell cycle regulation of myosin-V by calcium/calmodulin-dependent protein kinase II. *Science* 293, 1317–1320.
- Kennedy, M.B., Beale, H.C., Carlisle, H.J., and Washburn, L.R. (2005). Integration of biochemical signalling in spines. *Nat. Rev. Neurosci.* 6, 423–434.
- Khvotchev, M.V., Ren, M., Takamori, S., Jahn, R., and Sudhof, T.C. (2003). Divergent functions of neuronal Rab11b in Ca²⁺-regulated versus constitutive exocytosis. *J. Neurosci.* 23, 10531–10539.
- Lang, C., Barco, A., Zablow, L., Kandel, E.R., Siegelbaum, S.A., and Zakharenko, S.S. (2004). Transient expansion of synaptically connected dendritic spines upon induction of hippocampal long-term potentiation. *Proc. Natl. Acad. Sci. USA* 101, 16665–16670.
- Langevin, J., Morgan, M.J., Sibarita, J.B., Aresta, S., Murthy, M., Schwarz, T., Camonis, J., and Bellaiche, Y. (2005). *Drosophila* exocyst components Sec5, Sec6, and Sec15 regulate DE-Cadherin trafficking from recycling endosomes to the plasma membrane. *Dev. Cell* 9, 355–376.
- Li, Z., Okamoto, K., Hayashi, Y., and Sheng, M. (2004). The importance of dendritic mitochondria in the morphogenesis and plasticity of spines and synapses. *Cell* 119, 873–887.
- Lin, S.X., Grant, B., Hirsh, D., and Maxfield, F.R. (2001). Rme-1 regulates the distribution and function of the endocytic recycling compartment in mammalian cells. *Nat. Cell Biol.* 3, 567–572.
- Lisman, J.E., and Harris, K.M. (1993). Quantal analysis and synaptic anatomy—integrating two views of hippocampal plasticity. *Trends Neurosci.* 16, 141–147.
- Lledo, P.M., Zhang, X., Sudhof, T.C., Malenka, R.C., and Nicoll, R.A. (1998). Postsynaptic membrane fusion and long-term potentiation. *Science* 279, 399–403.
- Lu, W., Man, H., Ju, W., Trimble, W.S., MacDonald, J.F., and Wang, Y.T. (2001). Activation of synaptic NMDA receptors induces membrane insertion of new AMPA receptors and LTP in cultured hippocampal neurons. *Neuron* 29, 243–254.
- Luscher, C., Xia, H., Beattie, E.C., Carroll, R.C., von Zastrow, M., Malenka, R.C., and Nicoll, R.A. (1999). Role of AMPA receptor cycling in synaptic transmission and plasticity. *Neuron* 24, 649–658.
- Malenka, R.C., and Nicoll, R.A. (1999). Long-term potentiation—a decade of progress? *Science* 285, 1870–1874.
- Maletic-Savatic, M., and Malinow, R. (1998). Calcium-evoked dendritic exocytosis in cultured hippocampal neurons. Part I: trans-Golgi network-derived organelles undergo regulated exocytosis. *J. Neurosci.* 18, 6803–6813.
- Maletic-Savatic, M., Malinow, R., and Svoboda, K. (1999). Rapid dendritic morphogenesis in CA1 hippocampal dendrites induced by synaptic activity. *Science* 283, 1923–1927.
- Matsuzaki, M., Ellis-Davies, G.C., Nemoto, T., Miyashita, Y., Iino, M., and Kasai, H. (2001). Dendritic spine geometry is critical for AMPA receptor expression in hippocampal CA1 pyramidal neurons. *Nat. Neurosci.* 4, 1086–1092.
- Matsuzaki, M., Honkura, N., Ellis-Davies, G.C., and Kasai, H. (2004). Structural basis of long-term potentiation in single dendritic spines. *Nature* 429, 761–766.
- Merrifield, C.J., Perrais, D., and Zenisek, D. (2005). Coupling between clathrin-coated-pit invagination, cortactin recruitment, and membrane scission observed in live cells. *Cell* 121, 593–606.
- Okamoto, K., Nagai, T., Miyawaki, A., and Hayashi, Y. (2004). Rapid and persistent modulation of actin dynamics regulates postsynaptic reorganization underlying bidirectional plasticity. *Nat. Neurosci.* 7, 1104–1112.
- Osterweil, E., Wells, D.G., and Mooseker, M.S. (2005). A role for myosin VI in postsynaptic structure and glutamate receptor endocytosis. *J. Cell Biol.* 168, 329–338.
- Ostroff, L.E., Fiala, J.C., Allwardt, B., and Harris, K.M. (2002). Polyribosomes redistribute from dendritic shafts into spines with enlarged synapses during LTP in developing rat hippocampal slices. *Neuron* 35, 535–545.
- Park, M., Penick, E.C., Edwards, J.G., Kauer, J.A., and Ehlers, M.D. (2004). Recycling endosomes supply AMPA receptors for LTP. *Science* 305, 1972–1975.
- Prekeris, R., Foletti, D.L., and Scheller, R.H. (1999). Dynamics of tubulovesicular recycling endosomes in hippocampal neurons. *J. Neurosci.* 19, 10324–10337.
- Racz, B., Blanpied, T.A., Ehlers, M.D., and Weinberg, R.J. (2004). Lateral organization of endocytic machinery in dendritic spines. *Nat. Neurosci.* 7, 917–918.
- Ryu, J., Liu, L., Wong, T.P., Wu, D.C., Burette, A., Weinberg, R., Wang, Y.T., and Sheng, M. (2006). A critical role for myosin IIb in dendritic spine morphology and synaptic function. *Neuron* 49, 175–182.
- Shi, S.H., Hayashi, Y., Petralia, R.S., Zaman, S.H., Wenthold, R.J., Svoboda, K., and Malinow, R. (1999). Rapid spine delivery and redistribution of AMPA receptors after synaptic NMDA receptor activation. *Science* 284, 1811–1816.
- Skop, A.R., Bergmann, D., Mohler, W.A., and White, J.G. (2001). Completion of cytokinesis in *C. elegans* requires a brefeldin A-sensitive membrane accumulation at the cleavage furrow apex. *Curr. Biol.* 11, 735–746.
- Spacek, J., and Harris, K.M. (1997). Three-dimensional organization of smooth endoplasmic reticulum in hippocampal CA1 dendrites and dendritic spines of the immature and mature rat. *J. Neurosci.* 17, 190–203.
- Steiner, P., Sarria, J.C., Glauser, L., Magnin, S., Catsicas, S., and Hirling, H. (2002). Modulation of receptor cycling by neuron-enriched endosomal protein of 21 kD. *J. Cell Biol.* 157, 1197–1209.
- Sun, W., Yan, Q., Vida, T.A., and Bean, A.J. (2003). Hrs regulates early endosome fusion by inhibiting formation of an endosomal SNARE complex. *J. Cell Biol.* 162, 125–137.
- Tada, T., and Sheng, M. (2006). Molecular mechanisms of dendritic spine morphogenesis. *Curr. Opin. Neurobiol.* 16, 95–101.
- Terry-Lorenzo, R.T., Roadcap, D.W., Otsuka, T., Blanpied, T.A., Zamorano, P.L., Garner, C.C., Shenolikar, S., and Ehlers, M.D. (2005). Neurabin/protein phosphatase-1 complex regulates dendritic spine morphogenesis and maturation. *Mol. Biol. Cell* 16, 2349–2362.
- Toni, N., Buchs, P.A., Nikonenko, I., Bron, C.R., and Muller, D. (1999). LTP promotes formation of multiple spine synapses between a single axon terminal and a dendrite. *Nature* 402, 421–425.
- Toni, N., Buchs, P.A., Nikonenko, I., Povilaitite, P., Parisi, L., and Muller, D. (2001). Remodeling of synaptic membranes after induction of long-term potentiation. *J. Neurosci.* 21, 6245–6251.
- Triller, A., and Choquet, D. (2005). Surface trafficking of receptors between synaptic and extrasynaptic membranes: and yet they do move! *Trends Neurosci.* 28, 133–139.
- Ullrich, O., Reinsch, S., Urbe, S., Zerial, M., and Parton, R.G. (1996). Rab11 regulates recycling through the pericentriolar recycling endosome. *J. Cell Biol.* 135, 913–924.
- Yoshihara, M., Adolfsen, B., Galle, K.T., and Littleton, J.T. (2005). Retrograde signaling by Syt 4 induces presynaptic release and synapse-specific growth. *Science* 310, 858–863.